Synthesis of Nanophase Materials for Thermodynamically Tuned Reversible Hydrogen Storage

Channing Ahn, Sonjong Hwang, Justin Purewal
Caltech
June 9th, 2008

Project ID # STP21

This presentation does not contain any proprietary, confidential, or otherwise restricted information

Overview

Timeline

- Project start date:
  October 1, 2004
- Project end date:
  January 31, 2010

Percent complete: 60%

Budget

- Total project funding
  DOE share $1M (5 yrs)
  Contractor share $250k (5 yrs)
- Funding for FY07
  DOE share $200k
  Contractor share $50k
- Funding for FY08
  DOE share $200k
  Contractor share $50k

Barriers

(B) Weight and volume of on board hydrogen storage systems

(M) Reversibility of high capacity solid state storage materials

(N) Kinetics (fueling/refueling times) associated with current solid state storage materials

Partners

Interactions/ collaborations:

John Vajo, HRL Laboratories
Ewa Rönnebro, Sandia Natl. Lab.
David Sholl, Georgia Tech.
Jason Graetz, Brookhaven Natl. Lab.
J.C. Zhao, GE/Ohio State Univ.
Terry Udovic, NIST
R. C. Bowman, Jr. JPL

METAL HYDRIDE CENTER OF EXCELLENCE

Objectives

- To understand if thermodynamically tractable reactions based on hydride destabilization, that should be reversible but appear not to be, are kinetically limited.
- To enable short hydrogenation times associated with refueling, that will require short solid-state and gas-solid diffusion path lengths.
- To address the problems associated with large, light-metal-hydride enthalpies (hydrogen fueling/refueling temperatures) and develop strategies to address thermodynamic issues surrounding the use of these materials through hydride destabilization. Systems of interest determined through “theoretical screening” by MHCoE partner members.
- To understand issues related to grain growth and surface/interface energies, which are vital in order to understand the kinetics of hydrogenation/dehydrogenation reactions.
- To follow up on previously studied reactions with phase identification via x-ray diffraction, NMR and transmission electron microscopy.

Technical accomplishments: The $ScH_2 + 2LiBH_4 \rightarrow ScB_2 + 2LiH + 5/2H_2$ System: *Experimental Assessment of Chemical Destabilization*[a]

- Destabilization reaction with ideal thermodynamic properties (DFT)
  - ΔH_{300K} = 34.1kJ/mol[b]
  - 8.91 wt% capacity
- Isothermal kinetic desorption measurments (450ºC)
  - 4.5 wt% desorption

- Powder XRD detects only LiH and ScH_2 crystalline phases in desorption product, i.e. no reaction under these conditions between ScH_2 and $LiBH_4$.
- Stability of ScH_2, ScB_2 plays critical role in determining overall kinetics.

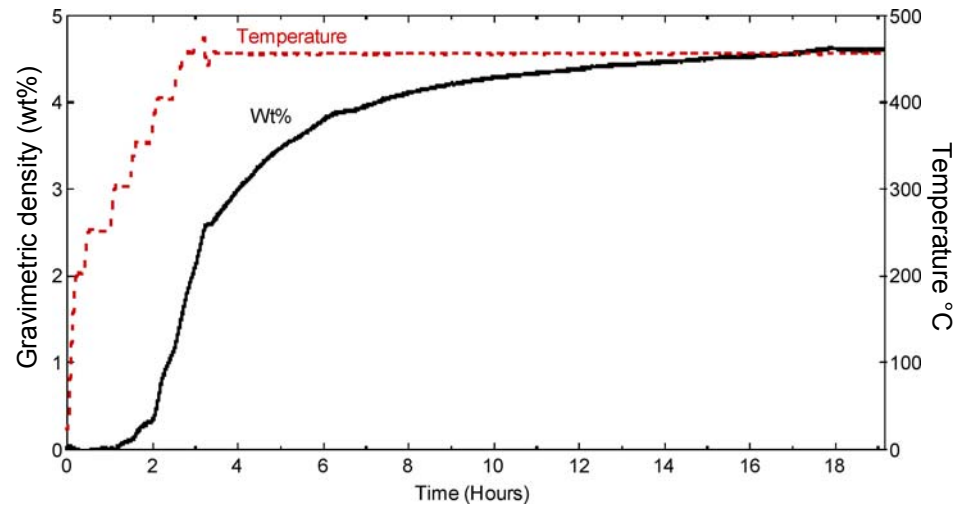

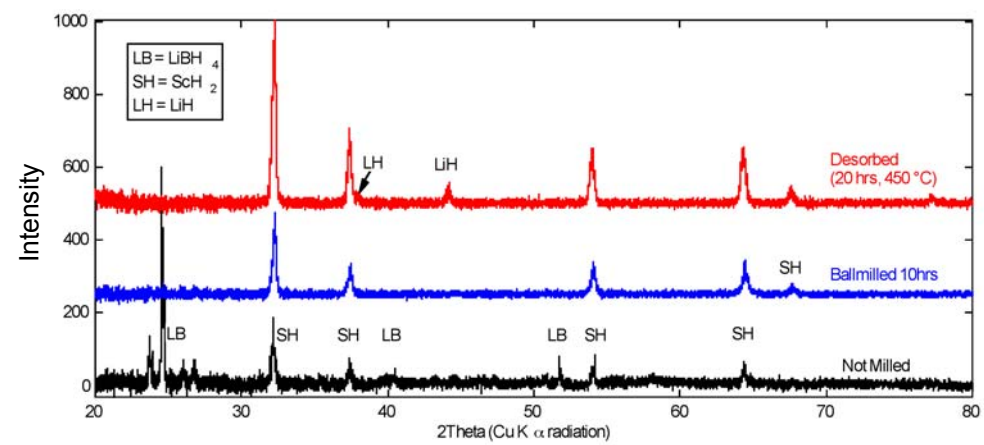

[a]Hydrogen Sorption Behavior of the ScH_2-$LiBH_4$ System: Experimental Assesment of Chemical Destabilization Effects, *Justin Purewal, Son-Jong Hwang, Robert C. Bowman, Jr., Ewa Rönnebro, Brent Fultz and Channing Ahn, accepted for publication in J. Phys. Chem. C (2008).*

[b]Calculated by Center partner David Sholl and published as Alapati, S. V.; Johnson, J. K.; Sholl, D. S., J. Alloys Compd. 2007, 446–447, 23.

Technical accomplishments: The ScH_2+2$LiBH_4$ → ScB_2 + 2LiH + 5/2H_2 System (continued): *MAS-NMR Spectroscopy*

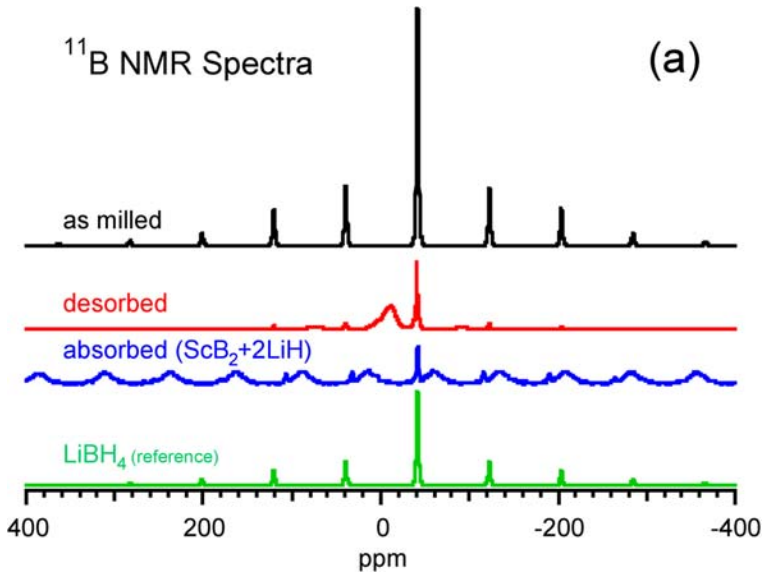

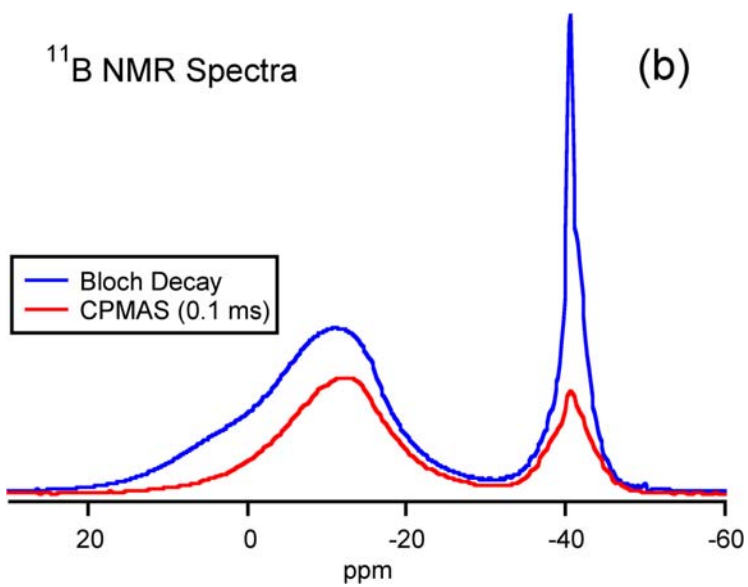

(a) Bloch decay ^{11}B MAS NMR spectra with neat $LiBH_4$ (Sigma-Aldrich) added as a reference. No change of $LiBH_4$ peak observed after ball milling. ^{11}B MAS and CPMAS spectra (a and b) show formation of elemental boron in the amorphous phase (broad shoulder at ~ 5 ppm) and formation of intermediate phase (with peak at -12 ppm), recently identified* as $[B_{12}H_{12}]^{2-}$ species. Note that a ^{11}B MAS NMR spectrum of ScB_2+2LiH system after absorption treatment at high H_2 pressure (896 bar, and 460°C for 48 hr) also included where the broader spinning sidebands in this spectrum are due to un-reacted ScB_2. The small peak at -41 ppm, indicates very limited $LiBH_4$ formation (~ 3%) in the reaction product. So reverse reaction is seen but under technologically challenging conditions.

(b) ^{11}B MAS and CPMAS NMR spectra (contact time=0.1 ms) of desorbed sample.

*NMR Confirmation for Formation of $[B_{12}H_{12}]^{2-}$ Complexes during Hydrogen Desorption from Metal Borohydrides, Son-Jong Hwang, Robert C. Bowman, Jr., Joseph W. Reiter, Job Rijssenbeek, Grigorii L. Soloveichik, Ji-Cheng Zhao, Houria Kabbour, and Channing C. Ahn, J. Phys Chem. C, 112, 3164-3169, 2008.

Technical accomplishments: The ScH_2+2$LiBH_4$ → ScB_2 + 2LiH + 5/2H_2 System (continued): *MAS-NMR Spectroscopy*

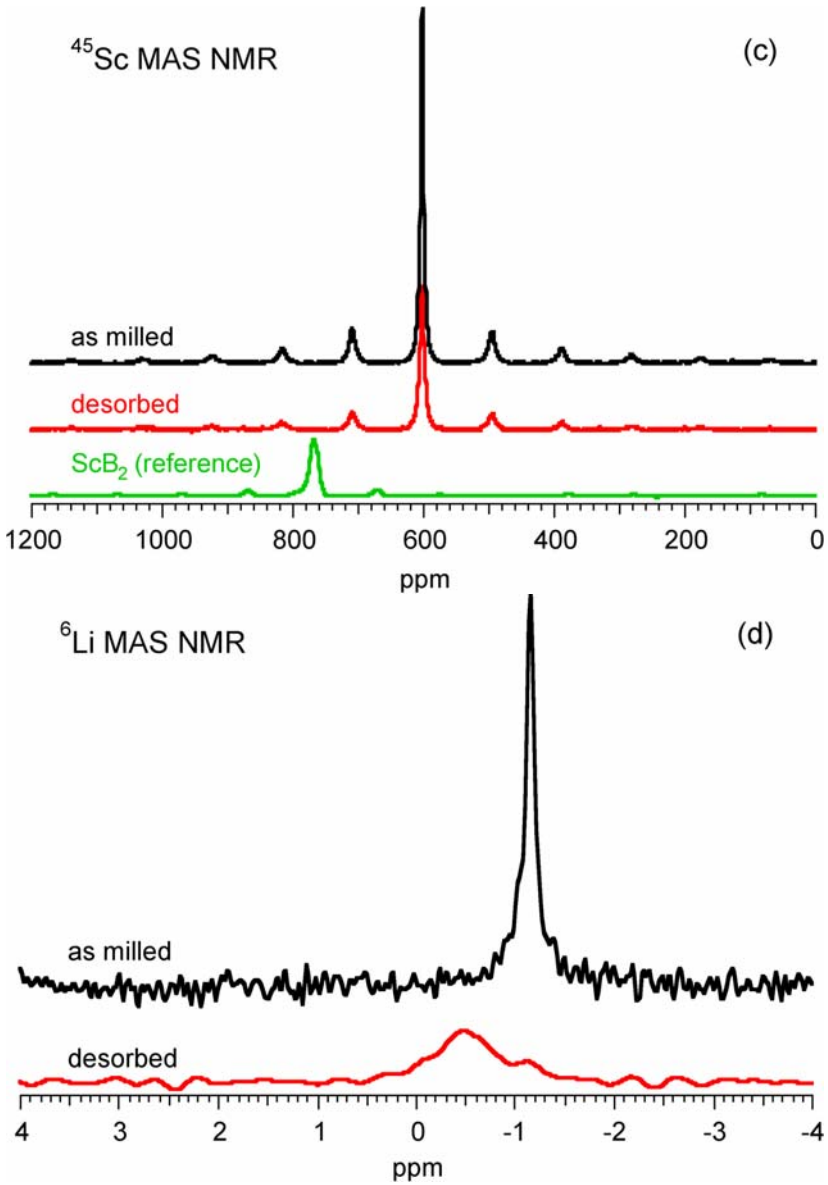

c) Un-reacted ScH_2 still present in desorption product, ScB_2/other Sc compounds not detectable in ^{45}Sc MAS NMR spectra presented in c). Note that ^{45}Sc MAS NMR signal significantly reduced after the desorption reaction, tentatively attributed to inhomogeneous separation of ScH_2 and $LiBH_4$ phases during the desorption reaction and correspondingly non-uniform distribution of ScH_2 particles in resulting NMR sample.

d) ^{6}Li MAS NMR spectra also show distinctive signature of phase changes from $LiBH_4$ (-1.1 ppm) to $Li_2B_{12}H_{12}$ (-0.5 ppm). Presence of LiH confirmed by independent ^{6}Li CPMAS NMR measurements (not shown) because extremely long spin lattice relaxation behavior inhibits observation during recording of MAS spectra. As with XRD data, NMR results identify decomposition products of $LiBH_4$, but show no evidence of ScH_2 reacting to form the ScB_2 product destabilization phase.

Technical accomplishments: The ScH_2+2$LiBH_4$ → ScB_2 + 2LiH + 5/2H_2 System (continued): *Raman Spectroscopy*

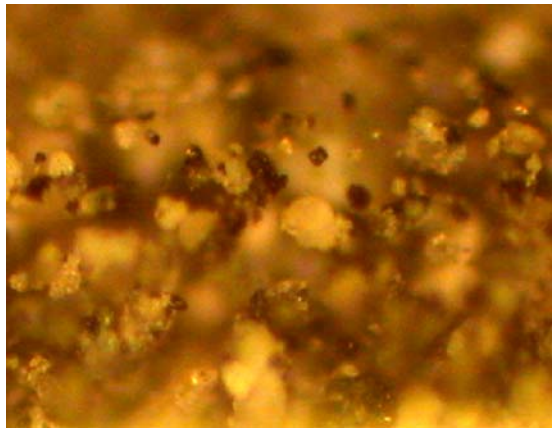

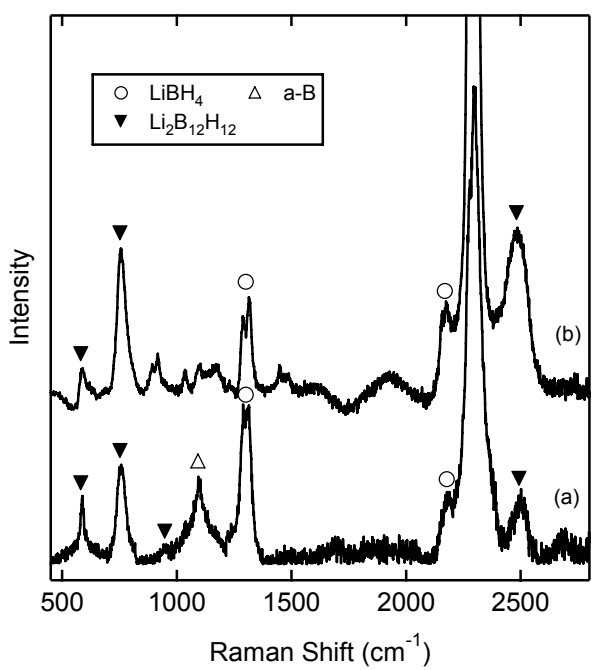

Top: Optical micrograph of a ScH_2+2$LiBH_4$ mixture after desorption at 400ºC for 20 hours. Desorption product segregates into two phases that are distinguished by their white and dark colors, respectively. The dark phase and the as-milled mixture not Raman active as determined by our spatially resolved analysis.

Bottom: White phase (trace a) shows similarities to the spectrum of dehydrogenated $LiBH_4$ (trace b). The B-H bending and stretching modes of $LiBH_4$ around 1300 and 2300 cm^{-1} present in both samples, and not affected by decomposition at temperatures below 400ºC. The broad peak at 1100 cm^{-1} corresponds to Raman modes from B-B bonding in amorphous boron. The additional B-H bending and stretching modes around 500-1000 cm^{-1} and 2500 cm^{-1} consistent with calculated and measured B-H vibrational modes in $Li_2B_{12}H_{12}$. These results suggest that the ball-milled ScH_2+2$LiBH_4$ mixture segregates back into its initial components upon melting and solidifying of $LiBH_4$. The dark phase contains ScH_2 while the white phase contains $LiBH_4$ and its thermal decomposition products. The solid triangles, open circles, and open triangles identify modes from $Li_2B_{12}H_{12}$, $LiBH_4$, and amorphous boron respectively.

$LiBH_4$ reversibility in $Ca(AlH_4)_2$ - $2LiBH_4$

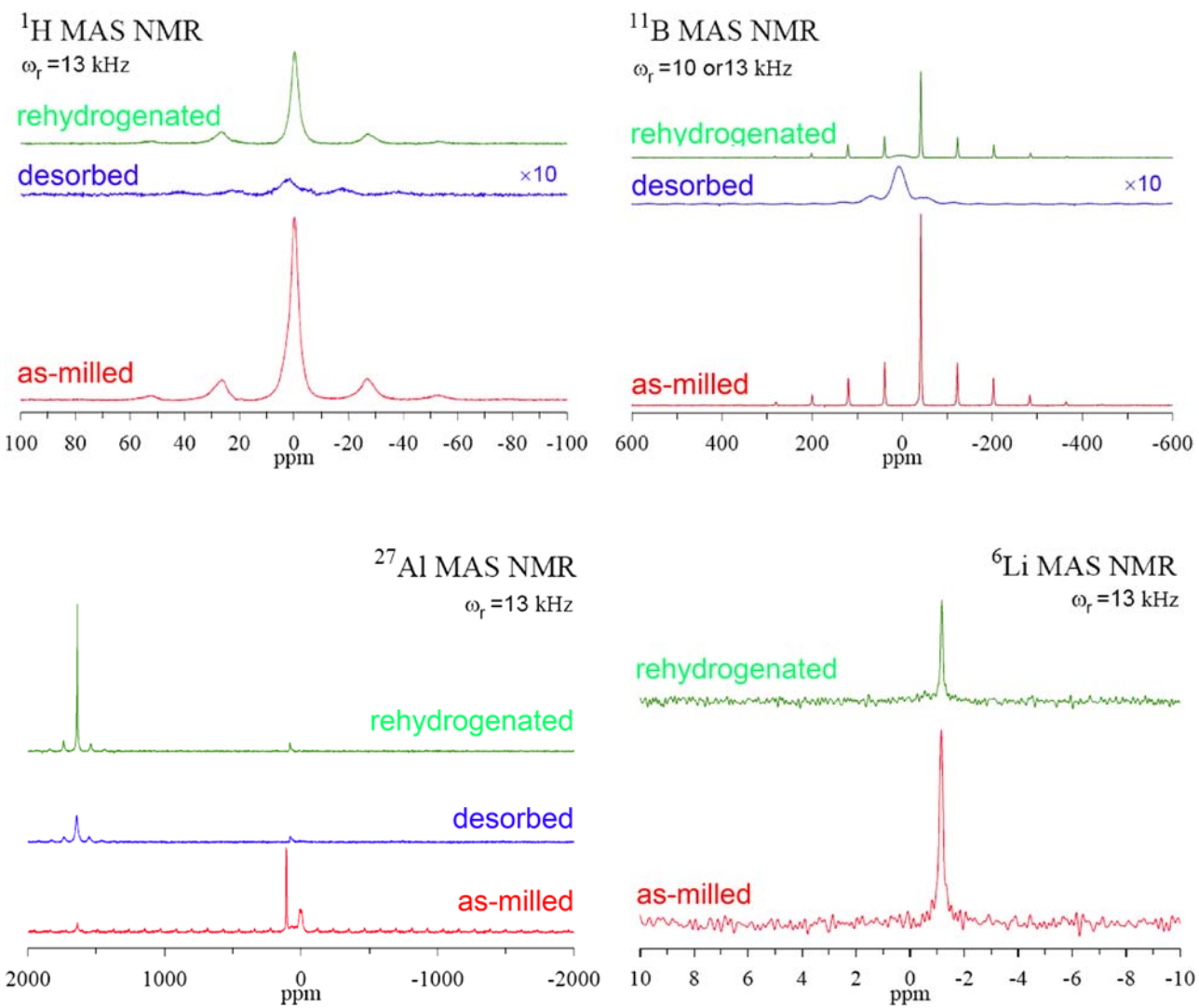

Proton, Li, B, Al NMR analysis of as milled, desorbed and rehydrogenated samples.

Initial work found partial reversibility in $LiBH_4$ when alanate made via mechano-synthesis* (~70% yield). ~88% $LiBH_4$ reversibility in $Ca(AlH_4)_2$-$2LiBH_4$ system although no evidence of CaB_2 formation. H, Li, and B NMR show that $LiBH_4$ can be rehydrogenated although the data for Al indicate that the $Ca(AlH_4)_2$ compound has undergone dissociation and the Al in this phase has transformed to the elemental state.

$LiBH_4$ reversibility in $Ca(AlH_4)_2$(pure)- $2LiBH_4$ cont'd

AlH_3 (reference)

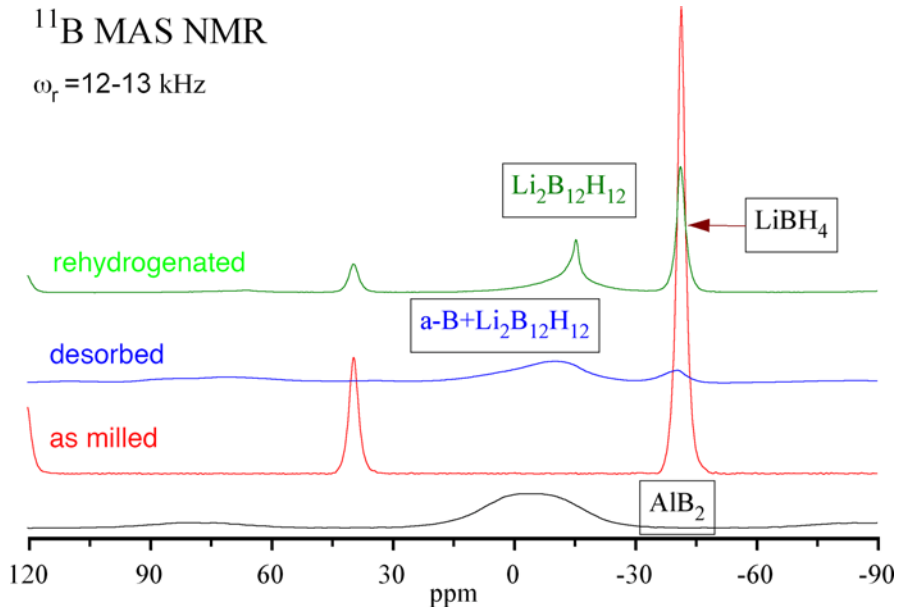

Solution synthesis $Ca(AlH_4)_2$

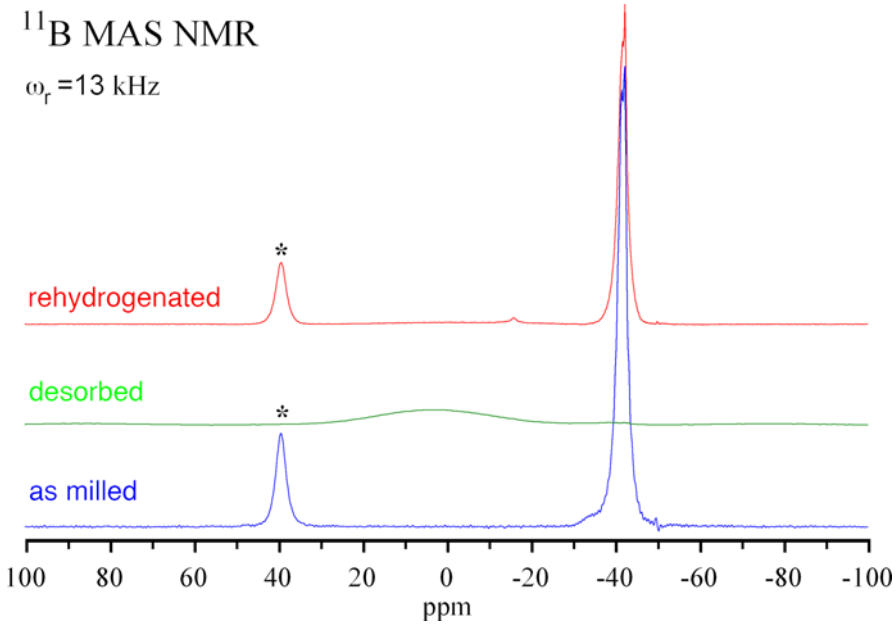

With ^{11}B MAS NMR, reversible formation of $LiBH_4$ is verified for 3 destabilization reactions containing aluminum hydrides.

Formation of $Li_2B_{12}H_{12}$ was also observed for all three systems. This is a competing reaction which limits reversibility of $LiBH_4$ formation.

$LiBH_4$ reversibility in AlH_3 - $2LiBH_4$ cont'd

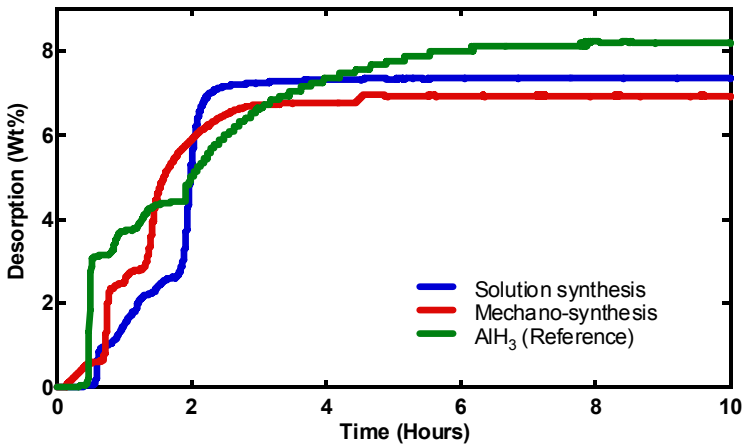

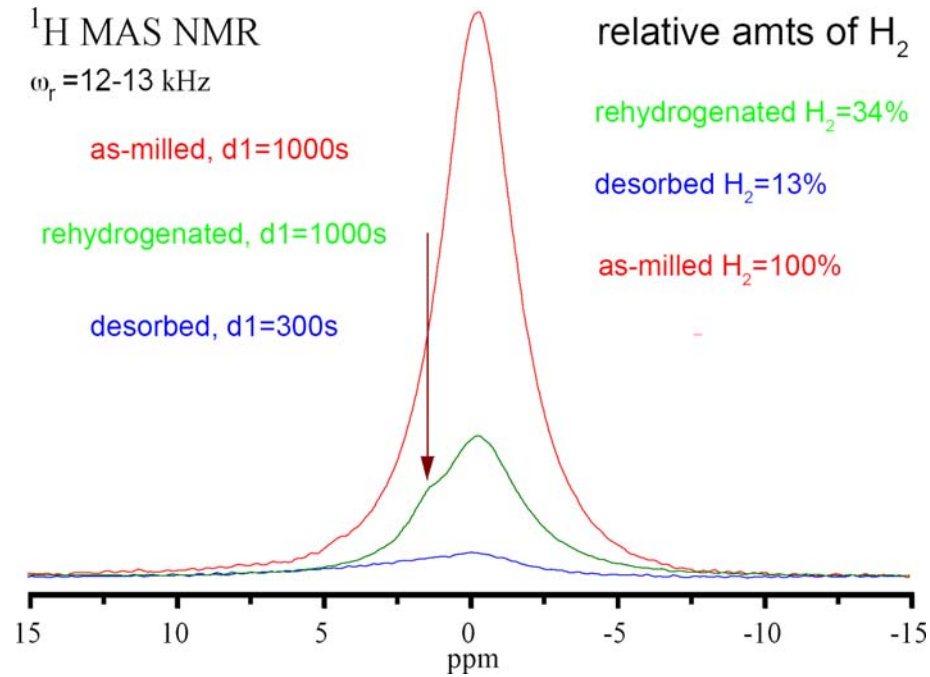

(above) Kinetic H_2 desorption data for a final temperature of 400°C. **(right)** ^1H MAS NMR revealing the H content in the direct synthesis of AlH_3 + $2LiBH_4$ system.

- $LiBH_4$ reversibly desorbs/reabsorbs H_2 when mixed with
  - $Ca(AlH_4)_2$ direct ball-milling synthesis
  - $Ca(AlH_4)_2$ synthesized in solution (pure)
  - AlH_3 (Dow Chemical)
- Catalytic role of elemental Al is key in reversible formation of $LiBH_4$

$LiBH_4$ reversibility in $Ca(AlH_4)_2$ - $2LiBH_4$: XRD Qualitative Phase Analysis

Solution synthesis

$AlH_3 + 2LiBH_4$

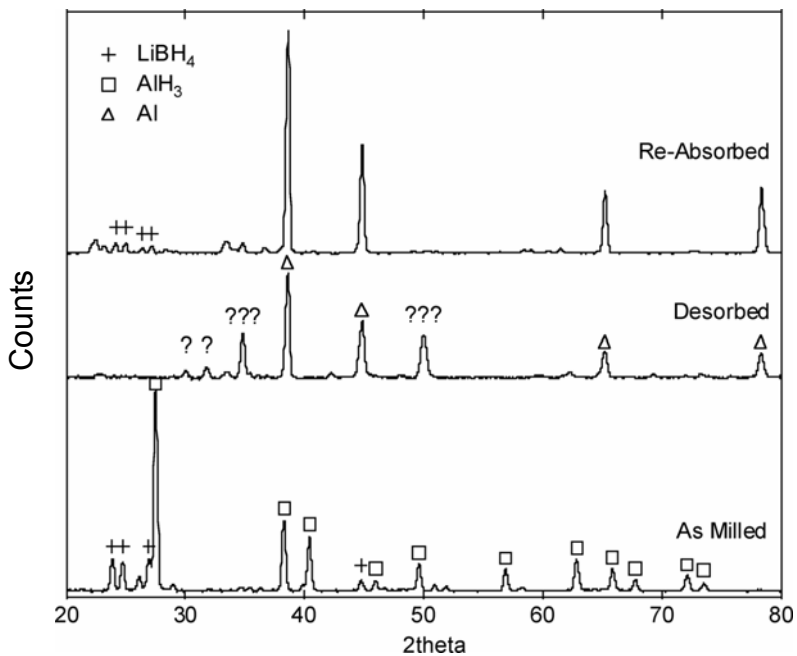

$Ca(AlH_4)_2 + 2LiBH_4$

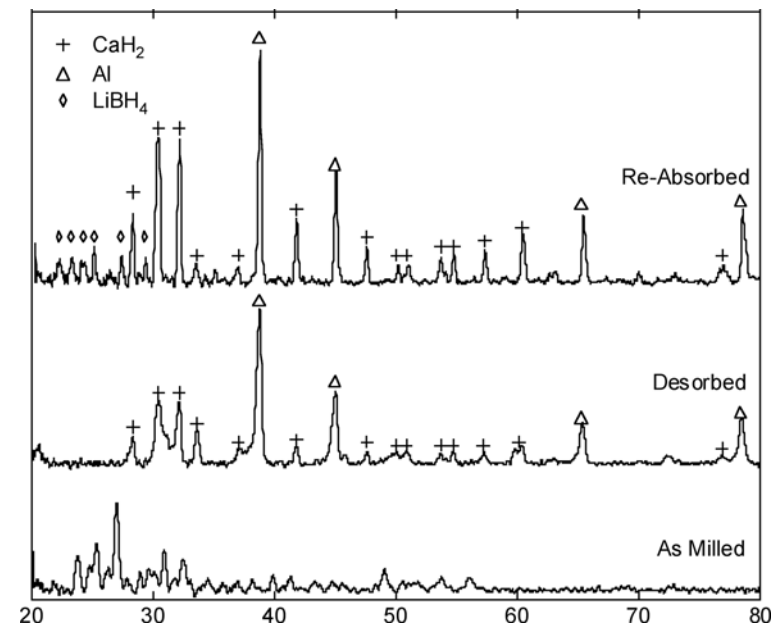

Formation of elemental aluminum is observed in all cases. Appears to have catalytic effect in reversible formation of $LiBH_4$. **(Right)** Formation of CaH_2 occurs as a side-reaction with $Ca(AlH_4)_2$. **(Left)** Peaks marked ??? have previously been identified as AlB_2 in the literature, but they don't match our reference pattern for AlB_2.

No data available yet for direct ball-mill synthesized $Ca(AlH_4)_2$

$LiBH_4$ reversibility in $Ca(AlH_4)_2$ - $6LiBH_4$

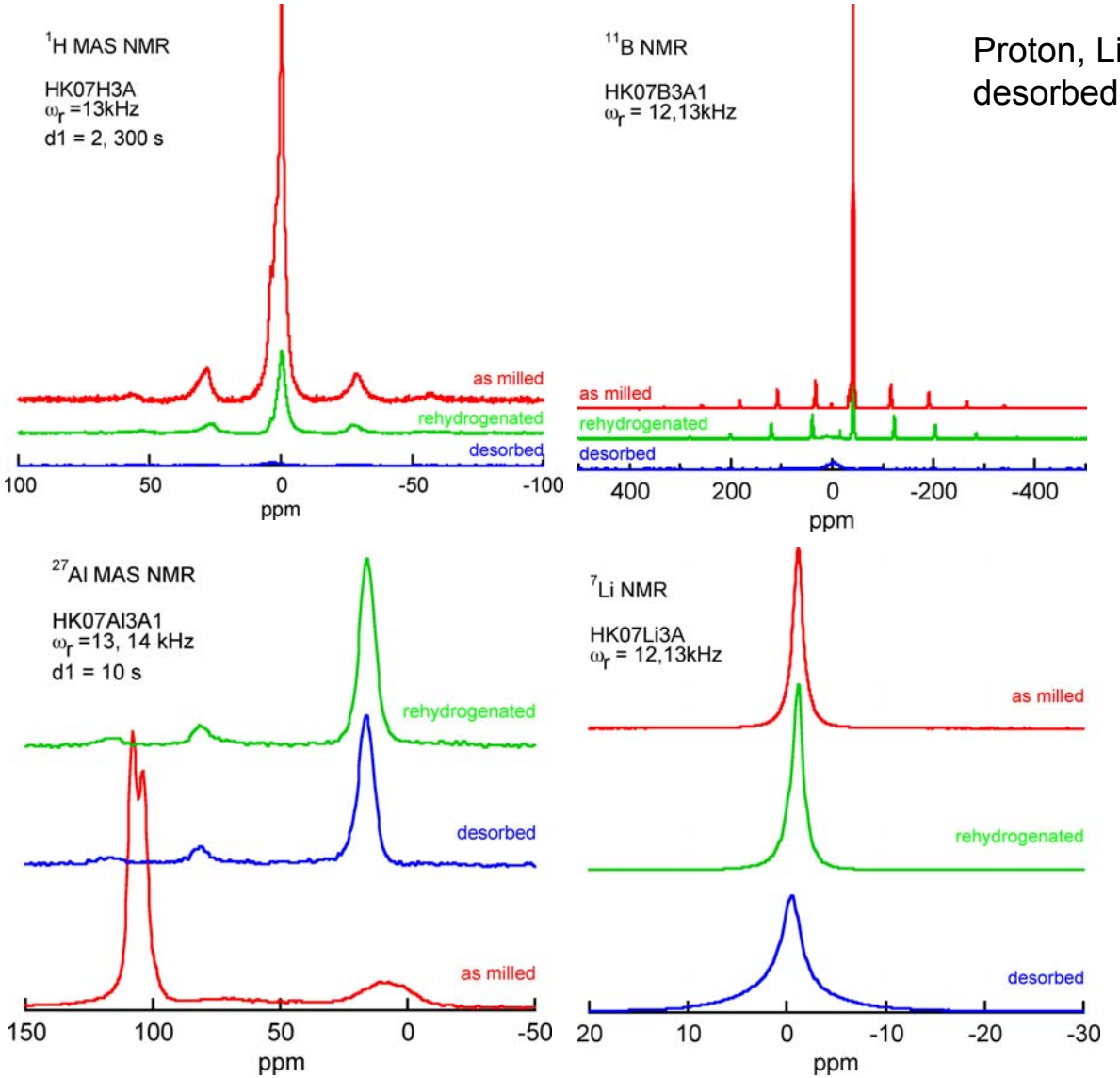

Proton, Li, B, Al NMR analysis of as milled, desorbed and rehydrogenated samples.

H desorbed and adsorbed in $LiBH_4$ in this system. ~40% $LiBH_4$ reversibility measured, less than in $2LiBH_4$ case. No NMR evidence of CaB_6 formation. $Ca(AlH_4)_2$ decomposes to Al metal. Formation of 981 and 782 ppm peaks in ^{27}Al NMR spectra of desorbed material observed for first time, but identities unknown.

Technical accomplishments:
Reaction pathways in borohydride systems

Direct thermal decomposition or destabilization system reaction pathways not easy to predetermine.

An important class of metal borohydride systems unexpectedly observed to produce a $(B_{12}H_{12})^{2-}$ intermediate phase as determined by NMR.

In collaboration with JPL and GE, $LiBH_4$, $Mg(BH_4)_2$, $LiSc(BH_4)_4$, $Ca(AlH_4)_2$-$LiBH_4$, studied by ^{11}B magic angle spinning and cross-polarization magic angle spinning as described in table below.

TABLE 1: Reactions Examined[a]

reaction	reactants	pretreatment	T_{desorb}/P_{final} [in total vessel volume]	H_2 desorbed (wt % of total sample)
1	$LiBH_4$ (Sigma Aldrich)	as received	400, 500 °C, 620 Torr [1.1 liters] or vacuum	varied
2	$Mg(BH_4)_2$	after second desorption	450 °C, ramp heating in vacuum	11.5
3	$ScCl_3$+3$LiBH_4$	ball milled	450 °C, ramp heating, 10351 Torr [24.4 cm^3]	7.7
4	$Ca(AlH_4)_2$+6$LiBH_4$	ball milled	350 C, 280 Torr [1.1 liters]	8.5

[a] Unless noted, pressures are final values, after desorbing into initially evacuated volumes. Quantity of desorbed H_2 is given as weight percent of original sample weight.

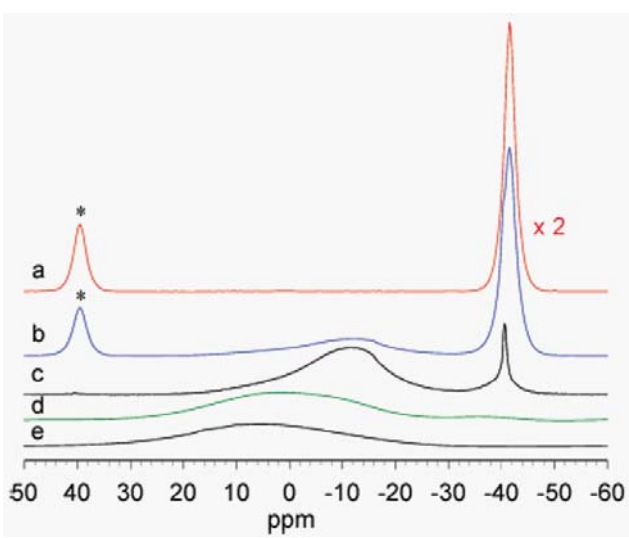

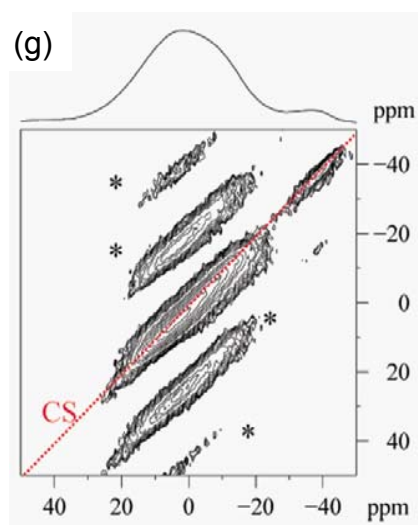

^{11}B NMR spectra at left, of powders collected after hydrogen desorption reactions of $LiBH_4$ (see Table 1). (a) $LiBH_4$ (as received, Sigma-Aldrich, note the scale adjusted by 1/2), (b) desorbed at 400°C, (c) desorbed at 500°C, (d) desorbed at 500°C under vacuum, (e) elemental boron in amorphous phase (Sigma-Aldrich), (g) ^{11}B MQMAS spectrum of sample d. Spinning side bands are marked with a *. The dashed line in 2D MQMAS spectra is the chemical shift axis.

Technical accomplishments:
(cont'd) *Reaction pathways in borohydride systems*

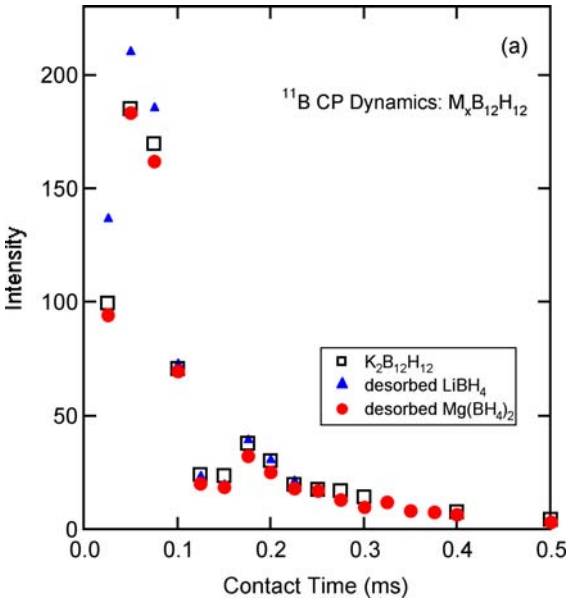

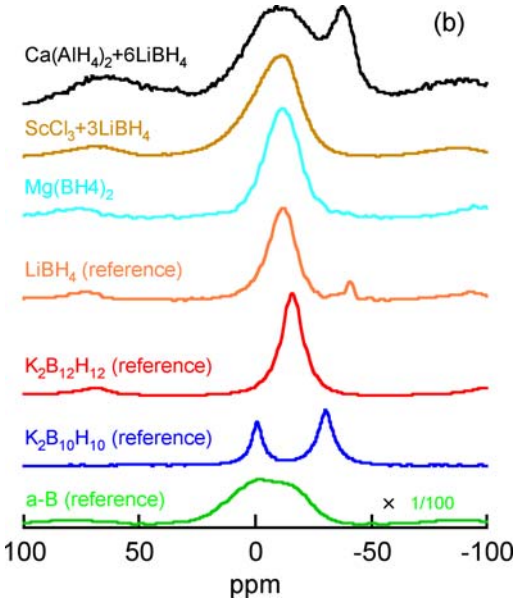

At left, (a) ^{11}B CPMAS variable contact experiment of powders collected after hydrogen desorption reactions of $LiBH_4$ and $MgBH_4$, and pure $K_2B_{12}H_{12}$. The broken line shows ^{1}H relaxation during the spin-lock period. (b) ^{11}B CPMAS NMR spectra of desorbed materials (see Table 1). The contact time of 0.05 ms was used. ^{11}B CPMAS spectra of elemental amorphous boron (a-B, note the scale change (1/100)), $K_2B_{10}H_{10}$, and $K_2B_{12}H_{12}$ reference compounds are added for comparison.

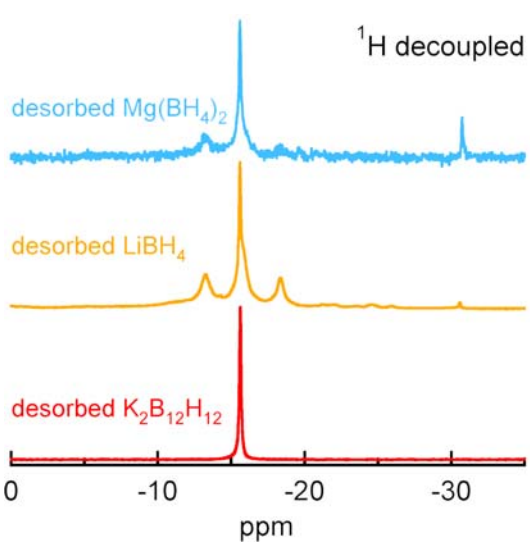

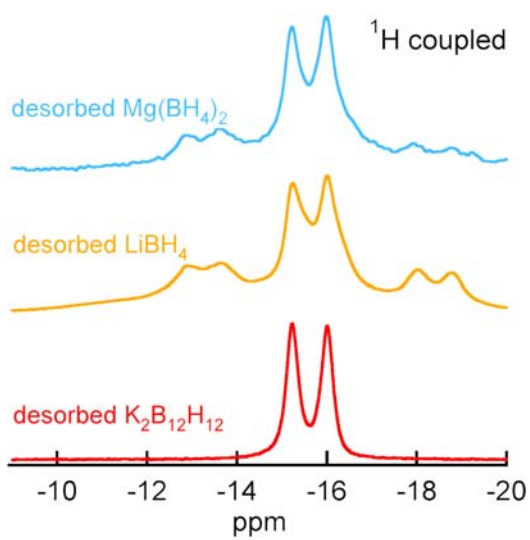

At left ^{11}B NMR spectra in solution phase after powders from desorption reactions were dissolved in H_2O. (c) ^{1}H decoupled, (d) ^{1}H coupled. Spectra from aqueous solutions of the $K_2B_{12}H_{12}$ compounds are compared to confirm the presence of $[B_{12}H_{12}]^{-2}$ unit in the dissolved $LiBH_4$ and $Mg(BH_4)_2$ decomposition products. J(B-H) was measured to be 125 Hz.

Technical accomplishments: Transmission electron microscopy and analysis of Mg in carbon aerogel

As part of an effort in looking into the possible effects of size on the thermodynamic properties of hydrogenation/ dehydrogenation, and in conjunction with HRL Laboratories, we have been looking at elemental distributions of Mg in carbon aerogels. Because of the lack of "wettability" of Mg on typical carbon surfaces (seen at right), schemes that promote the incorporation of Mg, especially into the small pore dimensions of aerogels needs to be verified.

Image at left shows attempt to melt Mg in carbon crucible and shows no evidence of wetting. Original ingot morphology was cylindrical and turned spheroidal with poor contact angle. Image at right shows similar attempt when Ni film of several hundred Å is deposited into crucible before melt attempt. Some Mg coating of surface evident, presumably from Mg vapor phase.

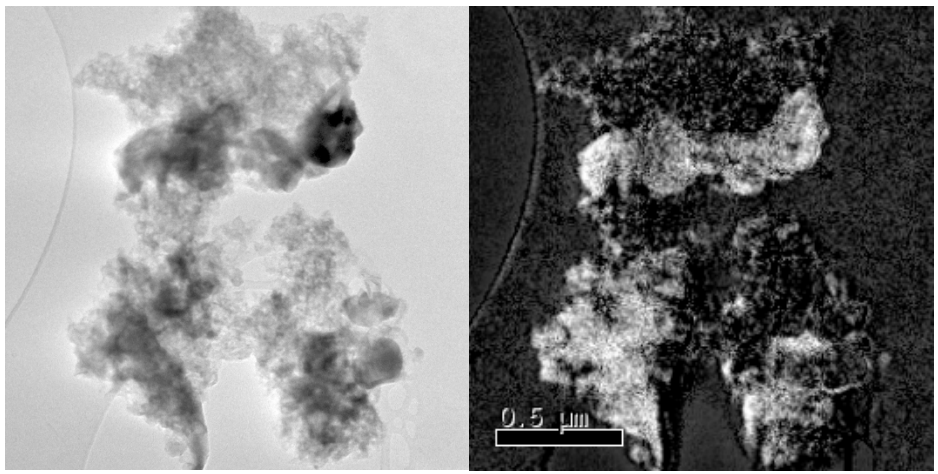

Sample 50559-60-1-c above showing aerogel clusters in bright field image at left. Mg image on right formed by using Mg L23 edge. The "white specular" regions are results of artifacts from difficulties with background subtraction. Region in upper right of these images shown in images at right (and rotated 90° anti-clockwise). Mg L23 image at 1/2 scale in upper right. Carbon K image at 1/2 scale in lower right.

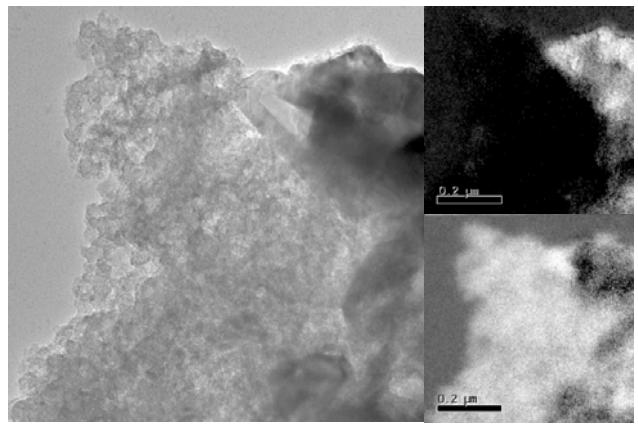

Technical accomplishments: Transmission electron microscopy and analysis of Mg in carbon aerogel cont'd

The typical microstructure can be dominated by regions of Mg metal or hydride that are decoupled from the aerogel regions as shown in the bright field image below,

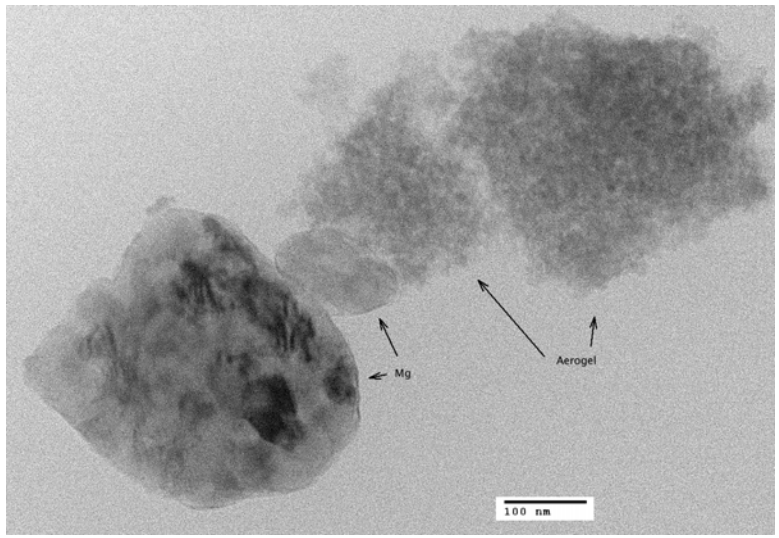

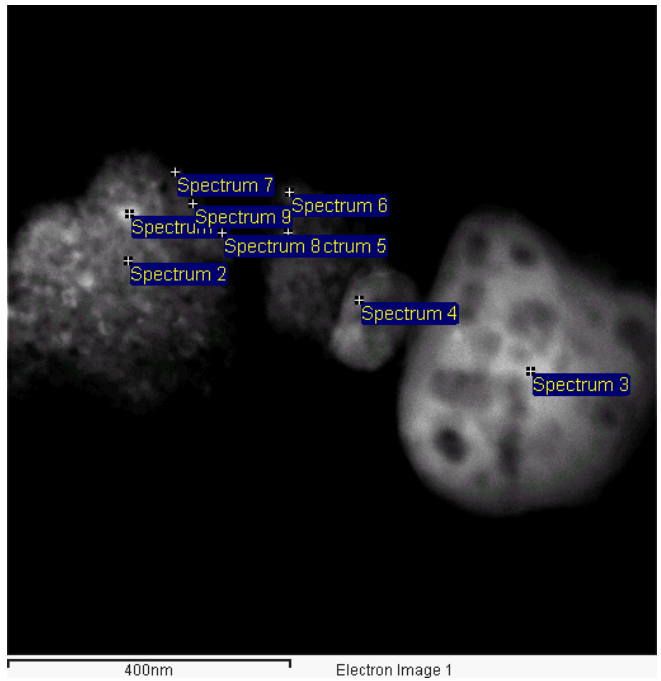

Characteristic of Mg particles in the aerogel microstructure are particles with smooth surfaces. To the upper right is high angle annular dark field image of the same region (where the bright regions are Rutherford scattered electrons with intensity that goes as Z^2) as above but where the image is inverted horizontally. While Mg_2Ni is commonly observed within the aerogel, the overall composition of typical aerogel regions is greater than this stoichiometry, indicating that excess Mg can be incorporated into the aerogel microstructure. While most of the Mg is found to go into larger pores, evidence for high Mg concentrations on the aerogel structure in nano phase form can be discerned.

Spectrum	In stats.	Mg	Ni
Spectrum 1	Yes	70.89	29.11
Spectrum 2	Yes	104.73	-4.73
Spectrum 3	Yes	99.94	0.06
Spectrum 4	Yes	100.30	-0.30
Spectrum 5	Yes	48.33	51.67
Spectrum 6	Yes	118.87	-18.87
Spectrum 7	Yes	52.81	47.19
Spectrum 8	Yes	94.51	5.49
Spectrum 9	Yes	88.85	11.15

All results in atomic%

FY 2008-09 plans

- Reaction path investigation in AlH_3 : $LiBH_4$ system to understand reversibility mechanism.
- Wetting and aerogel pore size enthalpy dependent studies.
- Continued NMR studies to identify reaction species that lack definitive crystallographic features.
- Enthalpy studies in micropore sized aerogels.
  - Pressure infusion approach to force metal/hydride into non-wetting pores.
- Coordination with T. Baumann (LLNL) in synthesis of aerogels with pore size range down to 1 to 2 nm. Surface/interface effects will play a dominant role in reaction enthalpy behavior at these size dimensions.
- Use of surface treatments/additives to enhance wetting of hydrides in aerogel pores.
- Confirmation of lowered enthalpies and diffusion paths in hydrides encapsulated within aerogel pores.